Simulation Study of MIG Welding Arc with Additional Magnetic Field Based on FLUENT

Qi Han, Shuyuan Jiang and Xiaowei Wang

Abstract A mathematical model of metal inert-gas (MIG) welding arc is established based on the theory of hydrodynamics and electromagnetism. The model is calculated with FLUENT fluid analysis software, UDS custom scalar equations, and UDF custom functions. Simulate the distribution laws of arc temperature field, arc plasma fluid velocity and arc pressure with or without additional magnetic field. Meanwhile, do experiments to validate the simulate results, and it is well consistent with the experimental results and measured results of the literature.

Keywords Welding arc · Additional magnetic field · MIG welding FLUENT

1 Introduction

As a new welding technique, the magnetic controlling welding has been deeply explored and studied by domestic and international workers [1–4]. But numerical simulation study in MIG welding arc with additional magnetic field is seldom reported. This paper takes MIG welding arc with additional magnetic field as object, and establishes a mathematical model. At the same time, use high speed camera system to observe and contrast the shapes and distributions of welding arc with different magnetic field intensity. The numerical simulation and experiments are combined to study the distribution laws of arc plasma fluid velocity, arc temperature and arc pressure, which provides the theoretical guidance for the control and improvement of magnetic controlling welding process.

Q. Han (✉) · S. Jiang · X. Wang
Institute of Aviation Manufacturing Engineering, Nanchang Hangkong University, 330063 Nanchang, China
e-mail: 1224348783@qq.com

S. Chen et al. (eds.), *Transactions on Intelligent Welding Manufacturing*,
Transactions on Intelligent Welding Manufacturing,
https://doi.org/10.1007/978-981-10-8740-0_10

2 Mathematical Model Foundation

2.1 Fundamental Assumption

The thermodynamic phenomena of the MIG welding arc with additional magnetic field is very complex. In order to simplify the calculation, the following assumptions are made when establishing the arc mathematical model: (1) the arc is symmetrical about the central axis and is in an incompressible state and in a pure argon atmosphere; (2) the arc plasma is in the local thermal equilibrium state (LTE); (3) the position of the wire end is unchanged relative to the flat work piece. And according to the literature [5], when the electrode end angle exceeds 60°, it begins to have an impact on the arc current density, ignoring the impact of the MIG welding droplet shape on the arc state; (4) the arc is optically thin, that is the re-absorption of the arc on the heat radiation is negligible with being relative to the heat loss of the arc; (5) the effect of droplet on the arc temperature field is ignored.

2.2 Control Equations

As a charged fluid, the magnetic controlling MIG welding arc is described and analyzed by magnetohydrodynamics theory. In the cylindrical coordinate system, the Navier-Stokes control equations, the energy conservation equation, and the Maxwell equations can be used to calculate welding arc plasma with the additional magnetic field.

Navier—Stokes control equations.

Quality continuity equation:

$$\frac{1}{r}\frac{\partial(r\rho v)}{\partial r} + \frac{\partial(ru)}{\partial z} = 0 \tag{1}$$

Axial momentum equation:

$$\begin{aligned}\frac{1}{r}\frac{\partial}{\partial z}(r\rho uu) + \frac{1}{r}\frac{\partial}{\partial r}(r\rho vu) = &-\frac{\partial P}{\partial z} + \frac{1}{r}\frac{\partial}{\partial r}\left[r\mu\left(\frac{\partial u}{\partial r} + \frac{\partial v}{\partial z}\right)\right] \\ &+ \frac{1}{r}\frac{\partial}{\partial z}\left[r\mu\left(2\frac{\partial u}{\partial z} - \frac{2}{3}\left(\frac{\partial u}{\partial z} + \frac{\partial v}{\partial r} + \frac{v}{r}\right)\right)\right] + F_z\end{aligned} \tag{2}$$

Radial momentum equation:

$$\frac{1}{r}\frac{\partial}{\partial r}(r\rho vv)+\frac{1}{r}\frac{\partial}{\partial z}(r\rho vu)=-\frac{\partial P}{\partial r}+\frac{1}{r}\frac{\partial}{\partial z}\left[r\mu\left(\frac{\partial u}{\partial r}+\frac{\partial v}{\partial z}\right)\right]$$
$$+\frac{1}{r}\frac{\partial}{\partial r}\left[r\mu\left(2\frac{\partial v}{\partial r}-\frac{2}{3}\left(\frac{\partial u}{\partial z}+\frac{\partial v}{\partial r}+\frac{v}{r}\right)\right)\right]+\rho\frac{u^2}{r}+F_r \tag{3}$$

Circumferential momentum equation:

$$\frac{1}{r}\frac{\partial}{\partial z}(r\rho uw)+\frac{1}{r}\frac{\partial}{\partial r}(r\rho vw)=\frac{1}{r}\frac{\partial}{\partial z}\left(r\mu\frac{\partial w}{\partial z}\right)$$
$$+\frac{1}{r^2}\frac{\partial}{\partial r}\left[r^3\mu\frac{\partial}{\partial r}\left(\frac{w}{r}\right)\right]-\rho\frac{vw}{r}+F_w \tag{4}$$

Energy conservation equation

$$\rho c_P\left(u\frac{\partial T}{\partial z}+v\frac{\partial T}{\partial r}\right)=\frac{\partial}{\partial z}\left(k\frac{\partial T}{\partial z}\right)+\frac{1}{r}\frac{\partial}{\partial r}\left(kr\frac{\partial T}{\partial r}\right)+Q \tag{5}$$

Maxwell equations.
Current continuity equation:

$$\frac{\partial}{\partial z}\left(\sigma\frac{\partial \varphi}{\partial z}\right)+\frac{1}{r}\frac{\partial}{\partial r}\left(\sigma r\frac{\partial \varphi}{\partial r}\right)=0 \tag{6}$$

Ohm's Law:

$$J\mathrm{r}=-\sigma\frac{\partial \varphi}{\partial r} \tag{7}$$

$$J\mathrm{z}=-\sigma\frac{\partial \varphi}{\partial z} \tag{8}$$

Ampere Circulation Law:

$$B_0=\frac{\mu_0}{r}\int_0^r J_z r d_r \tag{9}$$

where u is the axial (z) velocity; v is the radial (r) velocity; w is the circumferential (θ) velocity; ρ is the argon density; p is the static pressure; μ is the argon gas dynamic viscous coefficient; c_P is the argon heat capacity; σ is the argon gas conductivity; k is the thermal conductivity; T is the temperature; φ is the potential; J_r is the radial current density; J_z is the axial current density; B_0 is the arc self-induced magnetic field intensity; μ_0 is the vacuum permeability; F_z is the axial momentum source terms; F_r is the radial momentum source terms; F_w is the momentum source term; Q is the energy equation source term.

2.3 Boundary Conditions

Additional boundary conditions of magnetic controlling MIG welding arc models are shown in Table 1.

Where u_{giv} is the argon discharge rate; J_{giv} is the axial current density of the wire ends.

2.4 Gambit Pre-processing

Based on the assumptions made above, it is considered that the arc is symmetrical about the central axis and the three-dimensional arc problem can be transformed into a two-dimensional model grid. Use the pre-processing software Gambit to draw the model and mesh it. Among them, $(\mathrm{ar}-\mathrm{in})$ argon inlet is 3 mm; $(\mathrm{wall}-\mathrm{dzz})$ welding gun tip diameter is 3.5 mm; $(\mathrm{wall}-\mathrm{hs})$ wire length is 11.8 mm; (positive) wire radius is 0.6 mm; (axis) arc length is 6.8 mm. The model uses a regular quadrilateral structured grid to mesh it. Considering the arc temperature field and the gradient of the flow field in the bottom cylindrical region of the welding wire, the region grid is encrypted, the grid side length is 0.05 mm, the rest of the grid side length is 0.1 mm. The physical properties of argon vary with temperature; See the Ref. [6]. Figure 1 shows the arc calculation model and its meshing.

3 Results and Analysis

3.1 Arc Temperature Field Distribution

Figure 2 is the arc isothermal distributions with additional magnetic field intensity 0, 1.8, 3.6 mT. When the magnetic field intensity is 1.8 mT, the maximum

Table 1 Additional boundary conditions of arc model

Boundary name	Boundary type	u	v	w	T	φ
ar-in	Velocity inlet	u_{giv}	0	0	1000	$\frac{\partial\varphi}{\partial z}=0$
wall-ddz	wall	0	0	0	1000	$\frac{\partial\varphi}{\partial z}=0$
wall-hs	wall	0	0	0	1000	$\frac{\partial\varphi}{\partial r}=0$
Positive	wall	0	0	0	3000	$-\sigma\frac{\partial\varphi}{\partial z}=J_{giv}$
Axis	axis	$\frac{\partial u}{\partial r}=0$	0	0	$\frac{\partial T}{\partial r}=0$	$\frac{\partial\varphi}{\partial r}=0$
Negative	wall	0	0	0	6000	0
ar-out	Pressure outlet	$\frac{\partial u}{\partial r}=0$	$\frac{\partial v}{\partial r}=0$	$\frac{\partial w}{\partial r}=0$	1000	$\frac{\partial\varphi}{\partial r}=0$

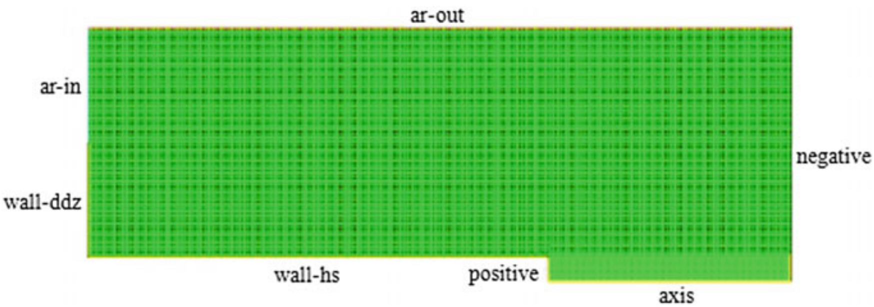

Fig. 1 Calculation and meshing model of arc

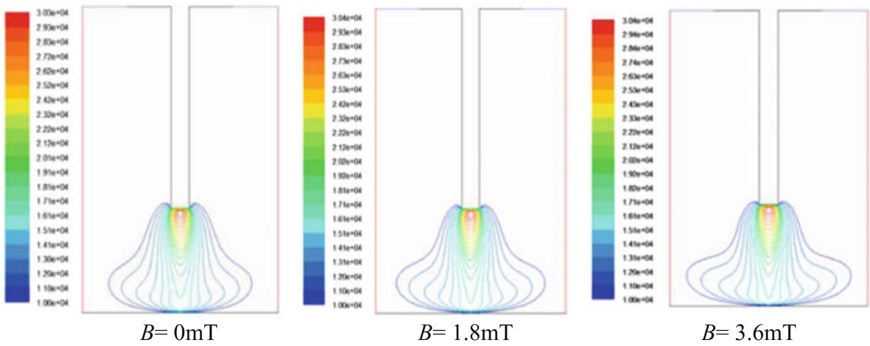

Fig. 2 Isothermal distributions of arc with different magnetic field intensity

temperature of the welding arc increases slightly. The changes of the welding arc shapes directly affect the temperature distributions of the arc. Relative to the absence of a magnetic field, arc isothermal line is the trend that the upper part is of contraction and the lower part is of extension; When the magnetic field intensity increases to 3.6 mT, this trend is more obvious. Compared with the ordinary MIG welding arc, the spiral movement of the charged particles with additional constant longitudinal magnetic field makes arc conduction current through the route increase, it is equivalent to increase the arc length and arc energy, so the arc temperature rises. Measure in real time GTAW welding arc temperature field with additional longitudinal magnetic field by thermal infrared imager in Ref. [7]. The simulation results of this paper are consistent with the measured in the literature, as shown in Fig. 3.

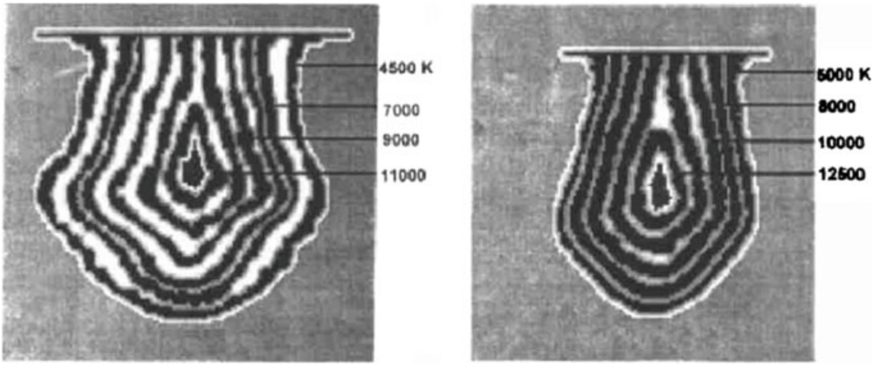

(a) B=10mT (a) B=0

Fig. 3 The measured temperature field of arc welding with a longitudinal magnetic field

3.2 Arc Plasma Fluid Velocity Distributions

In the case of an additional constant longitudinal magnetic field, the interaction of the charged particles in the radial motion direction with the longitudinal magnetic field produces the Lorentz force, causing the charged particles to rotate at high speed. Figure 4 is the arc plasma circumferential velocity distribution cloud.

With the 1.8 and 3.6 mT magnetic field intensity, the circumferential velocity of the welding arc has the same distribution characteristics. When the magnetic field intensity is 1.8 mT, the maximum rotational speed is 73.4 m/s. The magnetic field intensity increases to 3.6 mT, the circular rotational motion of plasma is more intense, the maximum speed is up to 136 m/s, and the rotational motion of the plasma has a greater radial extent due to the greater centrifugal force resulting from high-speed rotation. The centrifugal force causes the charged particles to converge to the edge of the arc column, resulting in charged particle density in the arc center

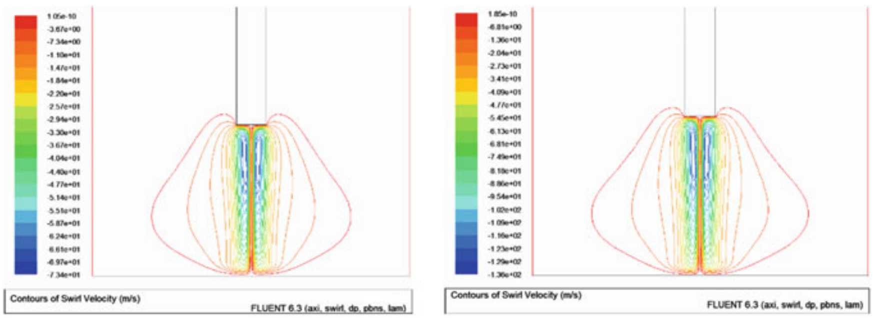

(a) B=1.8mT (b) B=3.6mT

Fig. 4 Welding arc plasma circumferential velocity distributions with magnetic field

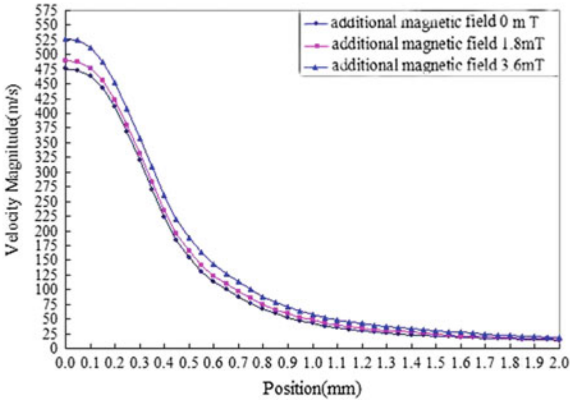

Fig. 5 Radial distribution of plasma velocity at arc cross Section 1 mm from the end of the wire

decreasing and the charged particle density at the edge of a region increasing. The region position is determined by the additional magnetic field intensity. The greater is the intensity of the additional magnetic field, the more intense is the rotational motion of the charged particles and the more obvious is the trend toward the edge. The area with the largest density of charged particles is farther away from the arc center axis.

The arc plasma velocities of the radial distribution curves are shown in Fig. 5 with different additional magnetic field intensity from the end of the wire at 1 mm.

The welding arc plasma velocity distribution along the radial direction has the same laws with the additional magnetic field intensity 0, 1.8 and 3.6 mT. The plasma velocity is highest at the center of the arc, and decreases gradually as the radial distance increases. Under the influence of the additional magnetic field, the velocity of the plasma movement is improved. Additional magnetic field intensities are 0, 1.8 and 3.6 mT, the plasma velocities at 1 mm from the end of the wire are 476, 490 and 527 m/s.

3.3 Arc Pressure Distributions

With the additional magnetic field, the arc pressure distributions have significant changes. Figure 6 shows the radial distributions of the arc pressure at a distance of 1 mm from the end of the wire with different additional magnetic field intensity.

The maximum value of the arc pressure at the central axis is 279 Pa without additional magnetic field. As the radial distance increases, the arc pressure decreases. With 1.8 mT additional magnetic field, the radial distribution of the arc pressure at 1 mm from the end of the wire changes significantly. The arc pressure at the arc axis is reduced. As the radial distance increases, the arc pressure increases first and then decreases, and has an arc pressure peak of 185 Pa at 0.25 mm from the center axis. When the additional magnetic field intensity increases to 3.6 mT, this trend is more obvious, the arc pressure of the central axis even becomes

Fig. 6 Radial distribution of arc pressure at 1 mm from the end of the wire

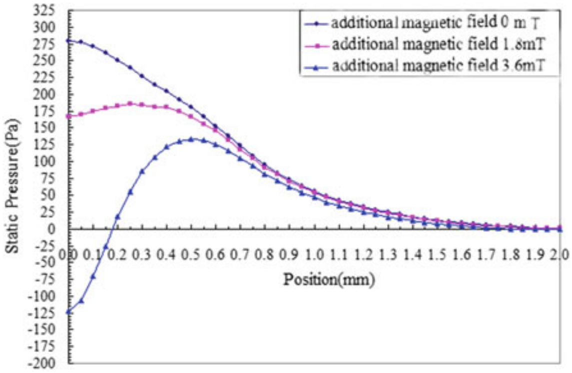

negative. At a distance of 0.5 mm from the axis, the maximum of the arc pressure is 133 Pa. Because the additional magnetic field makes the upper arc shrink, the range of the arc pressure is slightly smaller than that without the additional magnetic field. The simulation results are in good agreement with the experimental results of literature [8]. The above phenomenon is caused by the accumulation of charged particles to the edge of the arc, the number of particles in the arc column center is drastically reduced, the number of particles in the edge area increases, so the welding arc tends to be "hollow". This results in a decrease of the pressure in the arc center and a maximum of the arc pressure at a distance from the axis. When the additional magnetic field intensity reaches a certain value, the rotational motion of the arc plasma fluid will produce the so-called "whirlwind effect" [8]. The pressure at the central axis is further reduced or even negative.

4 Experimental Confirmations

Figure 7 is the collected arc shapes with different magnetic field intensity by a high-speed camera at the welding current 210 A, welding voltage 32 V, welding speed 0.54 m/min, argon flow 18 L/min, and it has good consistency with Figs. 2 and 4 simulation results.

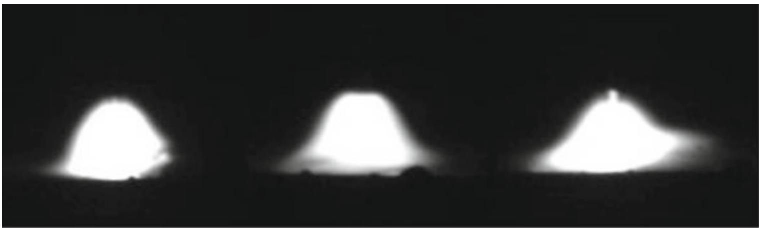

B=0mT *B*=1.8mT *B*=3.6mT

Fig. 7 MIG welding arc shapes with magnetic field intensity

Fig. 8 Distributions of measured arc pressure along the radial direction

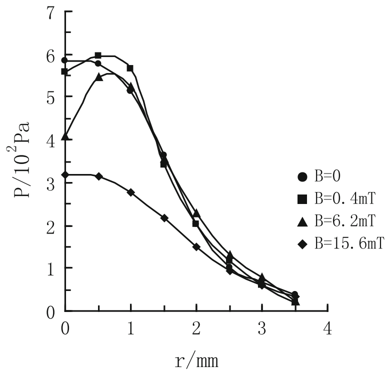

It can be seen from the Fig. 7 that the shapes of MIG welding arc change from conical to bell-shaped under the action of a constant longitudinal magnetic field. The changes of the welding arc shapes directly affect the arc temperature distribution and the arc pressure distribution, and distribution changes from a normal distribution to a bimodal distribution. When the additional magnetic field strength is 1.8 and 3.6 mT, the MIG welding arc shrinks in the upper part and expands in the lower part compared with no additional magnetic field. The arc shape is bell-shaped with axis-symmetry. The reason for this kind of arc shape changes is mainly due to the combined actions of the centrifugal force caused by arc rotation because of the interaction between the additional magnetic field and the arc charged particles and the pressure difference inside and outside the arc column.

Because MIG welding is a consumable electrode welding method, it is not suitable to measure the arc pressure distributions. In order to better study the effect of additional longitudinal magnetic field on welding arc, a small hole barometer is used to measure the arc pressure distributions of TIG welding.

Figure 8 is the measured radial distributions of the TIG welding arc pressure. For ordinary TIG welding ($B = 0$), the welding arc pressure is the largest and axis-symmetrical distribution at the center of the arc. With the longitudinal magnetic field, the center pressure of the TIG welding arc decreases and the maximum value is at some region of the arc edge. The arc pressure distributions have the same consistency with the simulation results in this paper.

5 Conclusion

(1) Establish the mathematical model of magnetic controlling MIG welding arc, and analyse the arc temperature field distributions, arc velocity field distributions and arc pressure distributions with FLUENT analysis software and UDF compilation.

(2) Simulate the distributions of arc plasma fluid field, arc temperature field and arc pressure. The results show that the distributions of arc temperature field are in good agreement with the measured data in the literature; The trend of arc pressure distributions are consistent with the test results.

Acknowledgements This paper is supported by the technology foundation of Jiangxi Province Department of Education (GJJ12434).

References

1. Jiang SY, Zheng XF, Chen HM et al (2004) The control mechanism of additional magnetic field on CO_2 welding splash. J Weld 25(3):65–67 (in Chinese)
2. Luo J, Ma J, Wang XJ et al (2009) Study of magnetic field on microstructure and crack behavior of magnesium alloy welds. Rare Metal Mater Eng 38(3):215–219 (in Chinese)
3. Chang YL, He YY, Du HZ et al (2007) Effect of longitudinal magnetic field on microstructure and properties of MIG welding of low carbon steel. J Shenyang Univ Technol 29(4):385–387 (in Chinese)
4. Hicken GK, Jackson CE (1966) Effects of applied magnetic fields on welding arcs. J Weld 45 (8):513–518
5. Lee SY, Na SJ (1996) A numerical analysis of a stationary gas tungsten welding arc considering various electrode angles. Weld J 75(9):269–279
6. Choo RTC, Szekely J, Westhofr RC (1992) On the calculation of the free surface temperature of gas-tungsten-arc weld pools from first principles. Part I: modeling the welding arc. Metall Trans B 23(3):357–369
7. Luo J, Jia CS, Wang YS et al (2001) The mechanism of GTAW welding with additional longitudinal magnetic field. J Metal 37(2):212–216 (in Chinese)
8. Luo J (1999) Study on fluid flow and heat transfer behavior of GTAW welding pool with longitudinal magnetic field. Dissertation. Xi'an Jiaotong University, Xi'an, China (in Chinese)